Bioorganic Chemistry 88 (2019) 102940

Contents lists available at ScienceDirect

Bioorganic Chemistry

journal homepage: www.elsevier.com/locate/bioorg

Phenanthroimidazole derivatives act as potent inducer of autophagy by activating DNA damage pathway

Hao Zhang[a,1], Yue Song[a,1], Li Li[b,c], Shuang-Yan Zhang[b,c], Qiong Wu[b,c,*], Wen-Jie Mei[b,c,d,*], Hui-Min Liu[a], Xi-Cheng Wang[a,*]

[a] The First Affiliated Hospital of Guangdong Pharmaceutical University, Guangzhou 510006, PR China
[b] School of Pharmacy, Guangdong Pharmaceutical University, Guangzhou 510006, PR China
[c] Guangdong Province Engineering Technology Centre for Molecular Probe and Biomedicine Imagining, Guangzhou 510006, PR China
[d] Guangzhou Key Laboratory of Construction and Application of New Drug Screening Model Systems, Guangdong Pharmaceutical University, Guangzhou 510006, China

ARTICLE INFO

Keywords:
Hepatocellular carcinoma
Autophagy
Apoptosis Inducer
Phenanthroline derivative
DNA damage
Zebrafish

ABSTRACT

A series of imidazo[4,5*f*][1,10]phenanthroline derivatives (**1–6**) have been synthesized in this study, and their inhibitory activity was evaluated by MTT assay. Results showed that all of these compounds demonstrate a promising inhibitory activity against a panel of human cancer cell lines. The **6**, the most effective compound with IC_{50} of approximately 2.3 ± 0.1 μM, was against the growth and could induce autophagy of HepG2 cells. This condition was confirmed by abundant autophagic vacuoles appearing in cells and evident ultrastructural changes observed under transmission electron microscopy. The autophage induced by **6** has also been demonstrated by up-regulating LC3-II and Beclin1. The apoptosis and G2/M phase cell cycle arrest through DSB damage have also been confirmed after the HepG2 cells were treated by **6**. These multiple effects, especially induction apoptosis and autophagy, indicate the potential of **6** for development as a novel anticancer drug.

1. Introduction

Hepatocellular carcinoma (HCC) is the major histological subtype of liver cancer and is the fifth most prevalent malignancy worldwide [1,2]. Despite recent therapeutic advancement, HCC has a poor prognosis with a high rate of mortality due to rapid recurrence and metastasis [3]. In China, HCC is the second most frequent cause of cancer-related mortality in males and the third in females [4,5]. Liver resection currently remains the most effective intervention modality with localized stage HCC. However, the majority of HCC patients are diagnosed at advanced stages with underlying liver dysfunction, thereby making the cure with resection treatment impossible [6–8]. In addition, treatment options among patients with unresectable HCC may include other palliative treatments, such as percutaneous ablation, TACE, cytotoxic chemotherapy, and three-dimensional conformal radiotherapy [9]. However, the effectiveness of these therapies needs further investigation [10–13]. Therefore, most patients rely on chemotherapy to prolong their lifespan. However, chemotherapy has shown low efficacy and unbearable side effects, thereby resulting in poor prognosis [14–17].

Autophagy, a type II programmed cell death, is a tightly-regulated catabolic process that involves the degradation of cytoplasm and cellular organelles via lysosomes [18–20]. In a tumor microenvironment, autophagy is a two-edged sword given that it is involved in cell survival and death [21–24]. Moreover, autophagy plays a major role in cell survival, growth, and homeostasis under hypoxic or metabolic stresses, and it becomes a cell survival pathway. Cellular stress can also lead to death itself once it is continuous or progressive. Therefore, autophagy could be positive or negative for cancer treatment depending on the environment [25–28]. The therapeutic target of the autophagic signaling pathway might be a novel molecular approach to kill cancer cells considering that autophagy is a fundamental process [29].

In recent decades, phenanthroline derivatives have attracted much attention because of their wide applications as duplex DNA-intercalating agents, molecular 'light switch', and antitumor chemotherapy drugs because of their unique capabilities as chelating agents [30–32]. In our previous studies, imidazo[4,5*f*][1,10]phenanthroline derivatives exhibited anticancer activity and induced tumor cell apoptosis via the NF-κB pathway [33]. Additionally, phenanthroimidazole derivatives have been further confirmed to act as potential inhibitors against various tumor cells by selectively targeting telomeric G-quadruplexes [34].

In this study, six novel imidazo[4,5*f*][1,10]phenanthroline derivatives (Scheme 1) have been synthesized with a yield of 87% under

* Corresponding authors.
E-mail addresses: wuqiongniu.1113@163.com (Q. Wu), wenjiemei@126.com (W.-J. Mei), 13902400598@126.com (X.-C. Wang).
[1] These authors contributed equally to the work.

https://doi.org/10.1016/j.bioorg.2019.102940
Received 31 December 2018; Received in revised form 21 March 2019; Accepted 18 April 2019
Available online 19 April 2019
0045-2068/

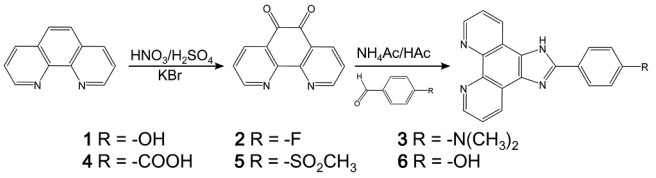

Scheme 1. The synthesis route of phenanthroimidazole derivatives under microwave irradiation.

microwave irradiation [35]. In addition, the derivatives' biological activities were further elucidated. During the investigation process, we found that **6** efficiently resists the growth of human hepatoma G2 cells. A surprise discovery, namely, autophagy, played a major role in the regulation of cell death. Thus, **6** is a promising agent as an autophagy inducer in the treatment of HCC. However, the potential molecular mechanism of the inhibiting cancer function of **6** remains obscure. Therefore, we designed a series of studies to explore the antitumor effect of **6** in human hepatoma G2 cells and to further elucidate its molecular mechanism.

2. Results and discussion

2.1. Biological activity

The antiproliferative activities of compounds **1–6** were evaluated using the MTT (3-(4,5-dimethylthiazol-2-yl)-2,5-diphenyltetrazolium bromide) assay, and the inhibitory activities (IC_{50}) of these compounds and cisplatin after 72-hour treatment are demonstrated in Table 1. The tested cancer cells, especially the HepG2 cell lines, exhibited a significant cytotoxic effect on the complexes. The IC_{50} of **6** against HepG2 cells is 2.33 μM, which is much less than that of cisplatin (93.09 μM).

2.2. In vivo inhibitory effect of 6 on zebrafish xenotransplanted liver cancer model

In decades, the zebrafish (*Danio rerio*) has been developed as a prominent disease model in various disease treatments before clinical research, especially in the field of tumor therapy [36,37]. Moreover, zebrafish is also permeable to many small molecules and thus potentially useful for drug screening. This study aims to further appraise the cancer-preventing effect of the most active compound **6** against HepG2 liver cancer cells *in vivo*. An experimental liver cancer xenograft model was used in this study to evaluate the inhibition on the growth of the HepG2 cells *in vivo*, and the fluorescence-labeled tumor cells were microinjected into the blood circulation of transgenic zebrafish (fli1:EGFP) embryos for 48 h. The hematogenous tumor cells were immediately disseminated in the embryo after injection near the subintestinal vessel (SIV) [38].

As shown in Fig. 1A, a certain amount of HepG2 cells were located near the SIV area in the zebrafish which dealt without drug at 0 h. However, an increasing number of tumor cells were distinctly observed after 48 h. HepG2 cells can infinitely proliferate in the zebrafish model [39]. Then, the number of HepG2 cells was slightly increased at 48 h over 0 h in the zebrafish after being treated with **6** (1 μM) (Fig. 1B). Furthermore, the number of HepG2 cells almost remain constant with a slight increase 48 h after treatment with **6** (3 μM), thereby indicating that this class of phenanthroimidazole derivatives, especially for **6**, can effectively suppress the proliferation of HepG2 cells in zebrafish. This compound can be developed as a potential agent to inhibit liver cancer.

2.3. Autophage of HepG2 cells induced by 6

2.3.1. Observation of autophagic vacuolization in cytoplasm by inverted phase contrast microscopy

The morphological characteristics of HepG2 cells treated with **6** were further observed by using an inverted phase contrast microscope. The normal control group's cells excellently adhered to smooth surface membrane, have a good refractive index, and show active nuclear fission. Remarkable morphological changes were observed when the tumor cells were treated with **6** for 24 h (Fig. 2A). Moreover, abundant autophagic vacuoles with varying sizes appeared, and cytoplasmic vacuoles progressively became larger and denser with increasing concentration of **6**. In addition, considerable cells treated with **6** at 3 and 5 μM concentrations became round, shrunken, and suspended at 24 h. Treatment of HepG2 cells with **6** remarkably showed a downward trend of the cell viability in a dosage-dependent manner (Fig. 2B)

2.3.2. Transmission electron microscopy

Transmission electron microscopy (TEM) was applied to detect the ultrastructural morphological changes of compound 6-treated HepG2 cells to further determine whether the cell vacuolization induced by 6 is involved in autophagy. The HepG2 cells untreated with 6 exhibited normal ultrastructural morphology of cytoplasm, organelles, and nuclei (Fig. 3A). The most prominent morphological change in 6-treated cells was the formation of abundant autophagic vacuoles sequestrating cytoplasm and organelles, such as mitochondria and endoplasmic reticulum. Double-membranes, giant autophagosomes filled with degraded organelles, and autolysosomes were frequently observed (Fig. 3B). TEM, the standard method for detecting autophagy, was performed to observe the formation of autophagosomes. Compound 6 could induce HepG2 cells to generate autophagy, which was consistent with the vacuolization obtained by inverted phase contrast microscopy.

2.3.3. Immunofluorescence microscopy

Cells were further analyzed by fluorescence microscopy. As shown in Fig. 4A, treatment of HepG2 cells with 0, 1, and 5 μM compound **6** displayed an increase in not only the number but also the size of MAP-LC3-positive points. This result indicated that **6** treatment induced the formation of autophagosomes.

Table 1
The inhibitory activity (IC_{50}/μM) of the target compounds against different cancer cells.

Comp.	Inhibitory activity IC_{50}/μM						
	MDA-MB-231	HepG2	EC-1	C6	MCF-7	A549	LO2
1	57.0 ± 0.2	8.6 ± 0.7	0.6 ± 0.8	16.3 ± 0.4	56.7 ± 0.9	6.3 ± 0.9	7.3 ± 0.2
2	89.0 ± 0.2	3.8 ± 0.9	68.0 ± 0.9	46.0 ± 0.3	4.4 ± 0.6	1.4 ± 0.9	1.1 ± 0.02
3	> 100	3.5 ± 0.9	20.0 ± 0.3	/	3.2 ± 0.9	1.3 ± 0.8	1.3 ± 0.3
4	57.5 ± 0.2	> 100	> 100	> 100	71.5 ± 0.9	7.2 ± 0.9	9.3 ± 0.6
5	65.6 ± 0.1	56.3 ± 0.8	22.0 ± 0.3	2.5 ± 0.3	42.2 ± 0.9	24.0 ± 0.8	13.7 ± 0.4
6	> 100	2.3 ± 0.9	20.0 ± 0.8	/	2.4 ± 0.9	13.0 ± 0.7	2.0 ± 0.07
cis-platin	17.8 ± 0.9	93.1 ± 0.9	/	/	76.9 ± 0.9	57.3 ± 0.7	13.5 ± 0.5

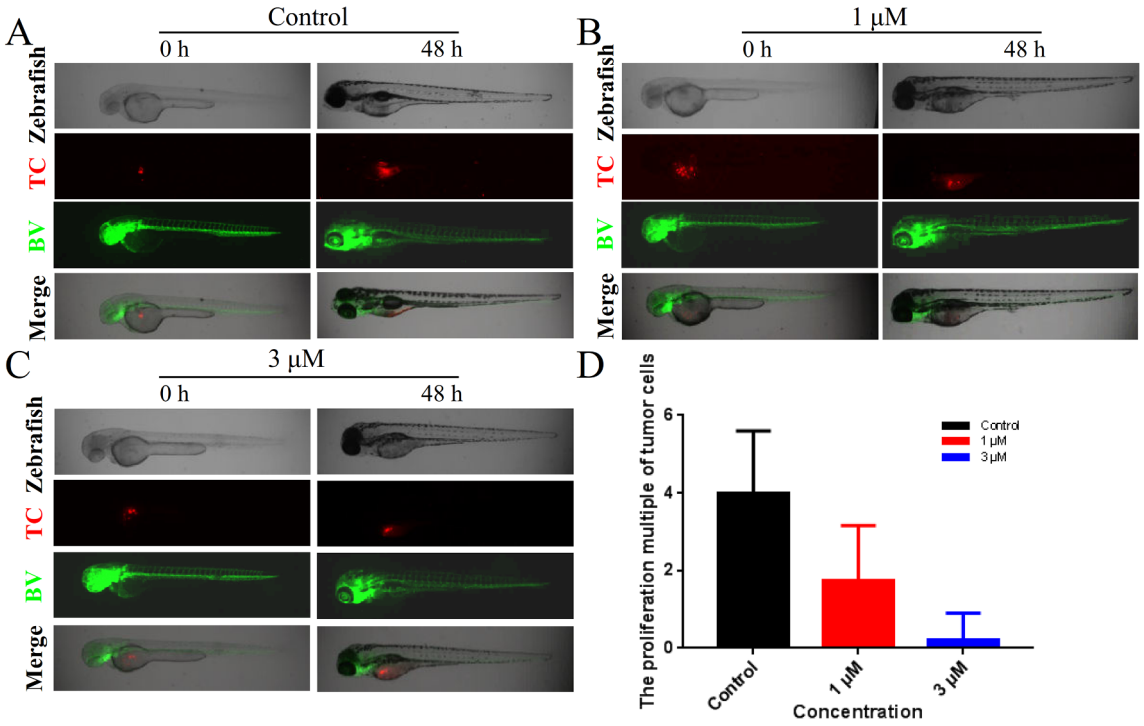

Fig. 1. (A) The growth inhibition of HepG2 cells induced by 6 in zebrafish xenografts model. Dil-labeled HepG2 cells (red) were microinjected into zebrafish embryos, and treatment with 6 (0, 1, 3 and 5 μM) for 48 h. (B) The proliferation multiple of tumor cells were analyzed through the fluorescence intensity of tumor cells at 48 h. The proliferation of the xenografts of HepG2 cells were imaged under a fluorescence microscope (n = 12/group).

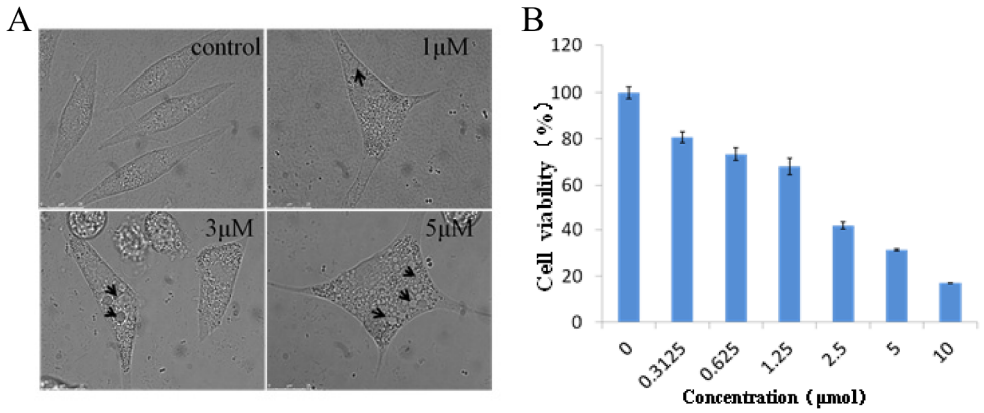

Fig. 2. (A) The morphological change of HepG2 cells in the absence and presence of **6**. (B) The cell viability of HepG2 cells induced by different concentration of **6**.

2.3.4. Western blot

First, we examined the expression of LC3, the mammalian homolog to the yeast Atg8 gene, via Western blot to further confirm the progression of autophagy. The LC3 protein can specifically label autophagosomal membranes, and the conversion of LC3-I to LC3-II is generally accepted as an autophagy marker [40]. During autophagic stress, the 16-kDa cytosolic form (LC3-I) is cleaved and post-translationally modified (LC3-II, 14 kDa) and translocated to the autophagosome [41]. After culturing HepG2 cells with compound 6 at 0, 1, 3, and 5 μM for 24 h, a remarkable increase in the ratio of LC3-II/LC3-I was observed compared with the vehicle-treated control. Additionally, treatment with 6 increased the ratio of LC3-II/LC3-I in a concentration-dependent manner (Fig. 4B). Beclin-1, one of the major autophagy-related gene (ATG) proteins, is the mammalian homolog of the yeast protein ATG6 that correlates directly with autophagic vesicle formation [42] and controls vital steps in the autophagic pathway. The Western blot analysis revealed the relative upregulation of Beclin-1 levels in a dose-dependent manner after 6 treatment. These results indicate that 6 can induce autophagy in HepG2 cells.

2.4. Apoptosis of HepG2 cells induced by **6**

A flow cytometric assay was used to distinguish the percentage of early and late apoptosis and necrotic cells by Annexin-V-FITC and PI double staining. The HepG2 cells were treated for 24 h with compound **6**. We monitor the changes of compound 6 on cell cycle perturbations considering the possibility that the induction of cell growth inhibition might be mediated through the regulation of the cell cycle. The cell cycle distribution was performed by flow cytometric analysis, as shown in Fig. 5A. After a 24-hour treatment, the G2/M phase population of the untreated cells was 2.2%, and the ratio of G2/M was considerably increased (6.2%, 11.2%, and 14.9% cells at 1, 5, and 10 μM concentrations of 6, respectively). The compound 6 treatment resulted in an appreciable arrest of HepG2 cells in the G2/M phase of the cell cycle

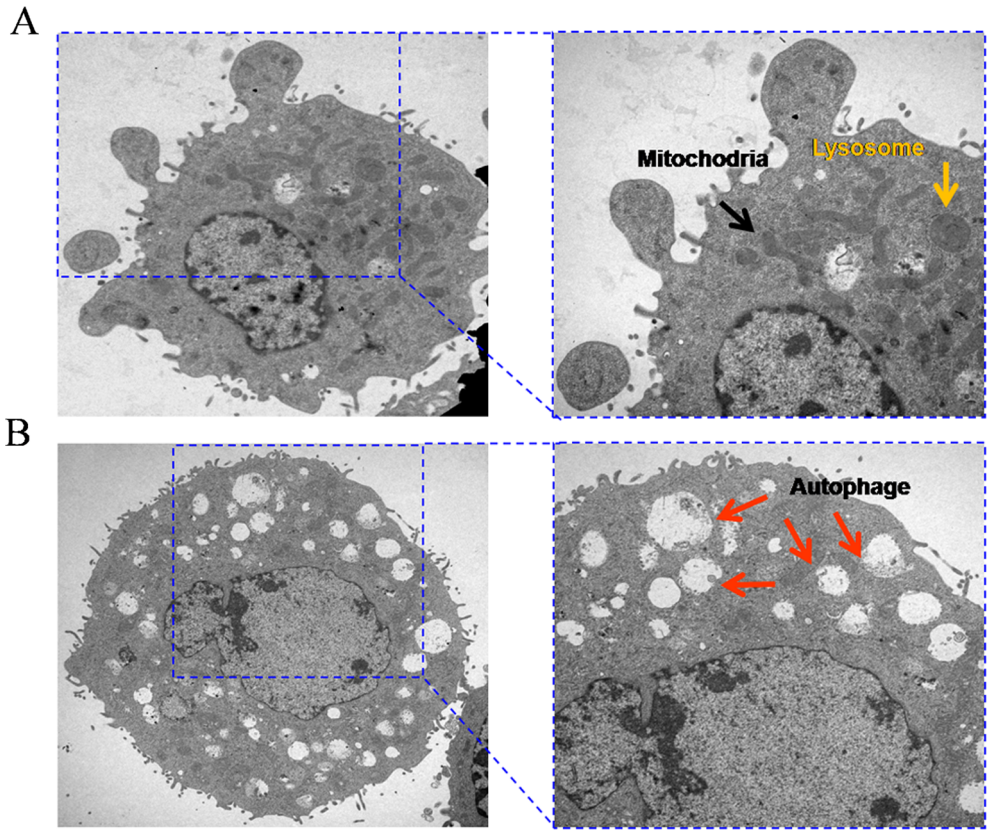

Fig. 3. Transmission electron microscopy showing the utophage process of HepG2 cells induced by **6**. (A) The ultramicroscopic structure of HepG2 cell without drug treatment. (B) The typical autophagic cells with many autophagic vacuoles (arrows) of HepG2 cells treated with compound 6 for 24 h.

compared with the control group. Specifically, this cell cycle accumulation at the G2/M phase after 6 treatment and the changes were concentration dependent. As shown in Fig. 5B, the percentages of early apoptotic were 18.80%, 22.42%, and 49.52% with 1, 5, and 10 μM treatment, respectively, whereas the proportion of untreated cells is only 1.15%. The result indicated that the **6** induced HepG2 cell apoptosis. Furthermore, the effect considerably increases in a dose-dependent manner. The DNA damage induction is an effective mode of action of anticancer agents. Anticancer agents act by producing sufficient DNA strand breaks in cancer cells to evoke cell repair systems, cell cycle arrest, or cell death programs [43,44].

2.5. DNA damage in HepG2 cells induced by *6*

Compared with the control, the increased expression and nuclear translocation of γ-H2AX, which is a sensitive central marker for DNA damage, were further confirmed by Western blot analysis [45,46]. Moreover, the expression of 6-induced γ-H2AX was markedly

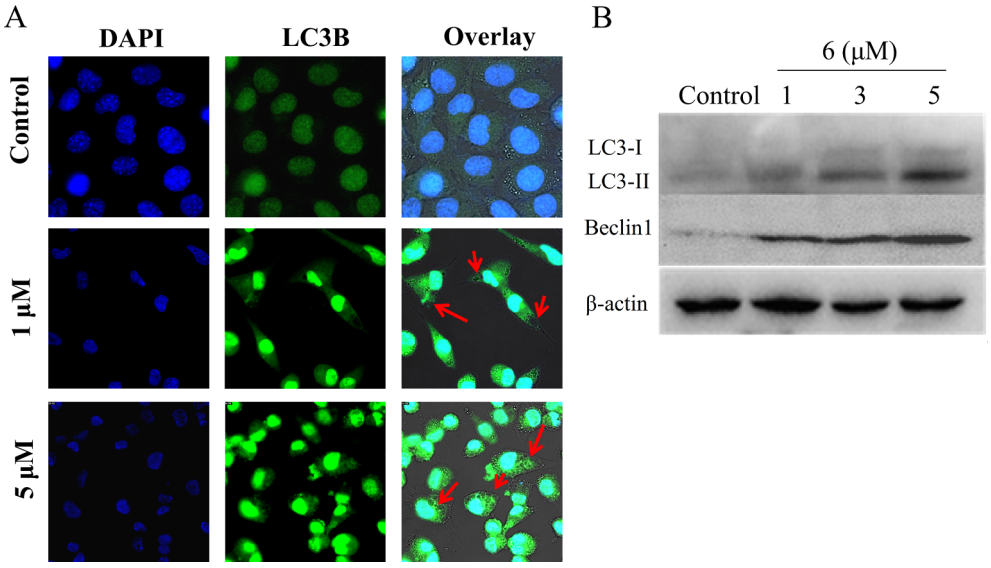

Fig. 4. (A) Fluorescence images of HepG2 cells showing endogenous MAP-LC3 levels examined by immunofluorescence staining. Nuclei (blue) were labeled by DAPI. (B) HepG2 cells were exposed **6** for 24 h. beclin1, LC3B, and β-actin levels were determined by Western Blot.

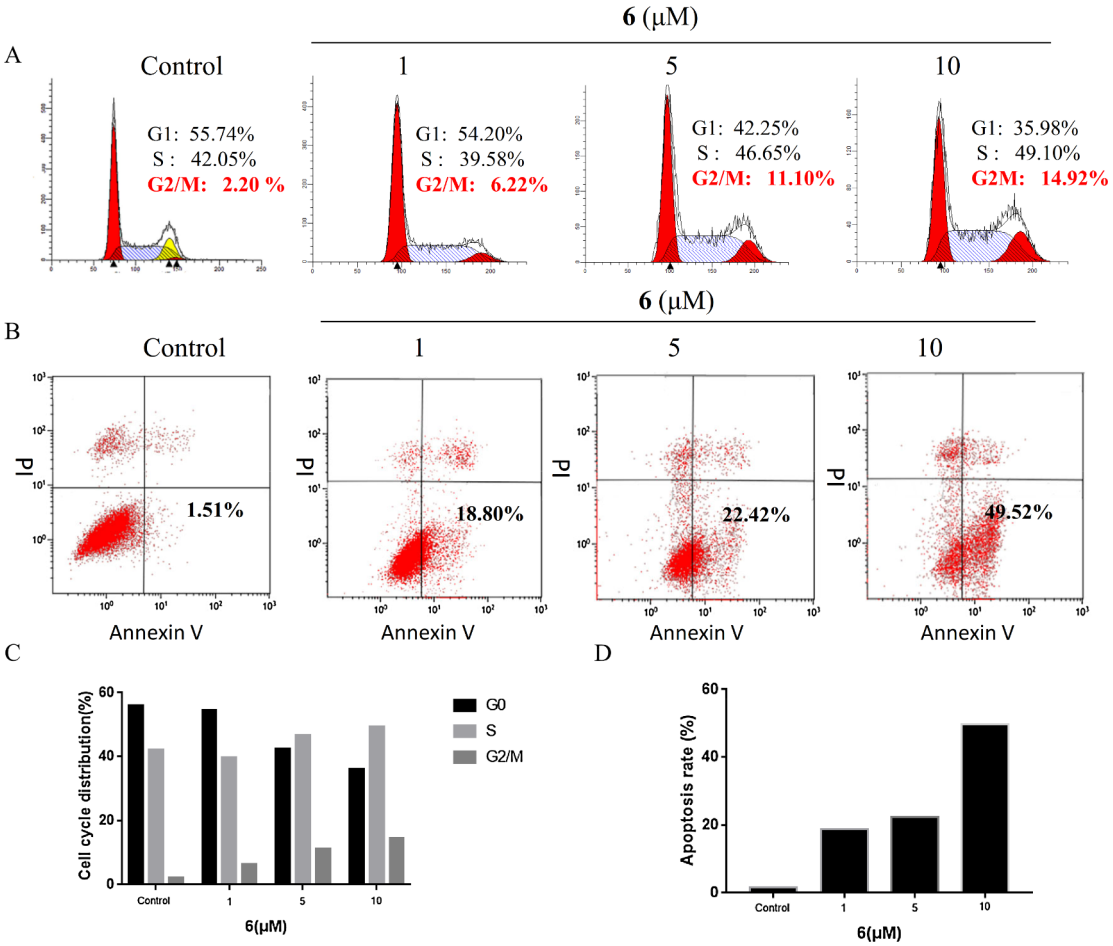

Fig. 5. (A) Flow cytometric analysis of HepG2 cells treated with **6** (0, 1, 5 and 10 μM) for 24 h. (B) Flow cytometric analysis for apoptosis after treatment by Annexin V-FITC and PI staining on HepG2 cells. After treatment with different doses of **6** (0, 1, 5 and 10 μM) for 24 h, apoptosis induction was observed. (C) Quantitative analysis of cell cycle distribution induced by different concentration of **6.** (D) The change of apoptosis induced by different concentration of **6.**

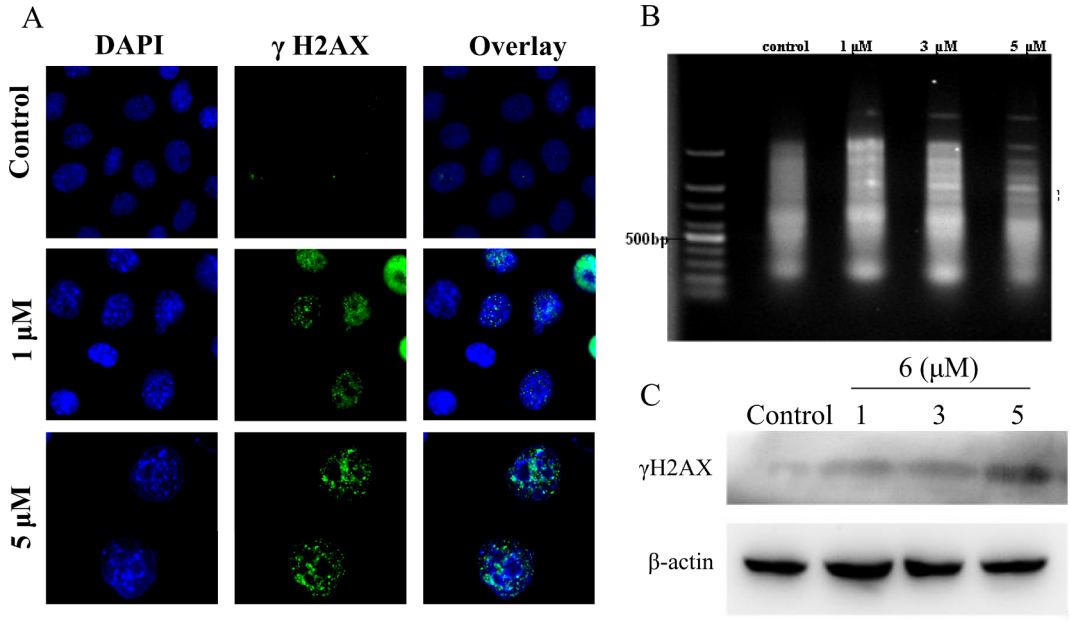

Fig. 6. (A) Cells were treated with compound 6 for 0, 1 and 5 μM, and translocation of γ-H2AX was detected by immunofluorescence staining. Cell nucleus was located by DAPI staining assay. (B) HepG2 cells treated with or without **6** for 24 h were visually detected DSBs using the DNA ladder assay; (C) HepG2 cells were exposed compound 6 for 24 h. γ-H2AX and β-actin levels were determined by Western blot.

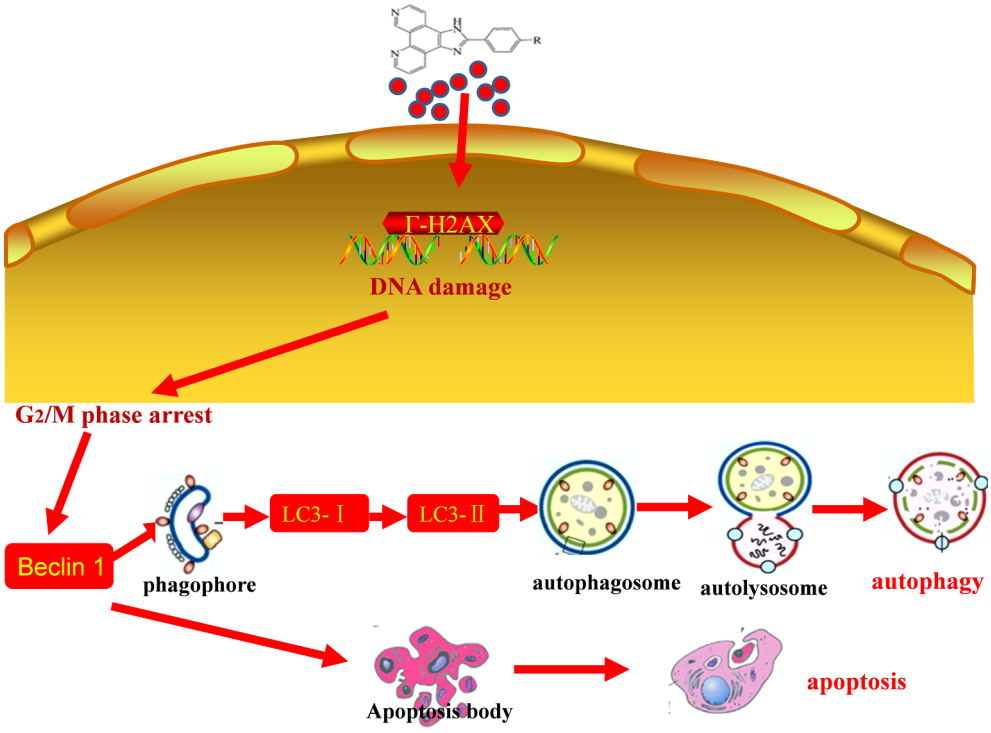

Fig. 7. A schematic depicting the role of compound 6 induced autophagy and apoptosis in HepG2 cells through DNA damage.

increased in a concentration-dependent manner at 24 h after treatment (Fig. 6A). We used the DNA ladder analysis by agarose gel electrophoresis to directly visualize the DSBs in tumor cells induced by **6**. This analysis reportedly detects DSBs induced by various DNA-damaging agents. DSBs in tumor cells were further tested. The reaction samples were separated by 1% agarose gel electrophoresis and visualized by UV light after standard ethidium bromide staining. As shown in Fig. 6B, the ladders in cells treated with **6** were more remarkable than those in untreated cells. On the basis of the above data, the **6** was determined as a novel DNA-damaging anticancer agent. Furthermore, a formation of γH2AX foci showed a dose-dependent increase in **6**-treated cells compared with control cells in the immunofluorescence assay (Fig. 6C).

As previously reported, imidazo[4,5*f*][1,10]phenanthroline derivatives induce apoptosis in cancer cells via suppression of NF-κB activity and down-regulation of c-myc gene expression. In this study, the phenanthroline derivatives successfully inhibited the cell proliferation of HepG2 cells, thereby activating autophagy and apoptosis. Moreover, the phenanthroline derivatives stimulated the DNA double-strand breaks in HepG2 cells, which play a critical role in mediating the G2/M phase transition, thereby leading to the accumulation of unrepaired DSBs and cell apoptosis. These increased DNA lesions might be due to the inhibition of DNA damage repair. Abundant cytoplasmic vacuoles were observed in **6**-treated HepG2 cells under an inverted phase contrast microscope. Moreover, the vacuoles were confirmed as autophagosomes by transmission electron microscopy, which is the "golden standard" for autophagy. According to the study, the treatment caused an increase of Beclin-1 and LC3-II expressions at the molecular level and resulted in cell apoptosis and autophagy (Fig. 7).

This study is the first to demonstrate that the capability of phenanthroline derivatives in initiating not only apoptosis but also autophagic cell death further promises an attractive strategy for developing advanced anticancer drugs. Moreover, phenanthroline derivatives are effective in therapeutic approaches for treating cancers to specifically target the autophagic cell death machine.

3. Conclusions

In conclusion, a series of imidazo[4,5*f*][1,10]phenanthroline derivatives exhibited high anticancer activities against several cancer cell lines. Compound **6** is identified as a potential antitumor agent and exerts its antineoplastic action by inhibiting cell proliferation and inducing cell apoptosis and autophagy. Autophagic cell death induced by **6** underlines its potential utilization as a new cancer treatment modality. In particular, autophagy may provide leverage to treat chemoresistant HCC on the basis of ineffective apoptosis.

4. Experimental section

4.1. Materials and method

All solvents and buffer fractions were of analytical and biology grades and used as received, respectively. Imidazo[4,5*f*][1,10]phenanthroline (Alfa Aesar), cisplatin (Acros), MTT (Sigma), Annexin V-FITC/PI (TOYOBO), and Trizol (Invitrogen) antibodies for detecting LC3B, Beclin-1, γ-H2AX, and *β*-actin were purchased from Santa Cruz. Microanalysis (C, H, and N) was performed with a vario EL elemental analyzer. The ^{1}H NMR spectra were recorded on a Varian INOVA 500NB NMR spectrometer with $(CD_3)_2SO$ as solvent at room temperature and TMS as the internal standard. Electrospray mass spectra were registered with a Thermo Finnigan LCQ DECA XP ion trap mass spectrometer, equipped with an ESI source. The ^{1}H and ^{13}C NMR spectra were recorded on a Varian-300 spectrometer.

4.2. Synthesis and characterization

Phenanthroimidazole derivatives were synthesized in accordance with the literature procedure with some modifications. Generally, a mixture of 1,10-phenanthroline-5,6-dione (1.50 mmol), benzaldehyde (2.25 mmol), ammonium acetate (51.9 mmol), and glacial acetic acid was heated at 100 °C for 20 min under microwave irradiation (Scheme 1). Then, 20 mL of water was added, and the pH value was adjusted to

7.0 at room temperature [47–49]. The solution was filtered and dried in a vacuum to obtain a yellow precipitate. The product was purified in a silica gel column by using ethanol as eluent. The target compounds were characterized by ESI-MS and ^{1}H- and ^{13}C NMR spectroscopy.

4.3. Cell culture

The A549 (lung adenocarcinoma), MDA-MB-231 (human breast cancer), MCF-7 (human breast cancer), EC-1 (esophageal cancer), L-02 (human normal liver), C6 (rat glioma cell), and HepG2 (human liver HCC cells) were obtained from the National Key Lab of Molecular Oncology, Cancer Institute and Cancer Hospital, Chinese Academy of Medical Science. All cell lines were cultured in DMEM media (Gibco, Gaithersburg, MD, USA) supplemented with FBS (10%), penicillin (100 units/ml), and streptomycin (50 units/ml) at 37 °C in a CO_2 incubator (95% relative humidity, 5% CO_2).

4.4. MTT assay

Cell viability was determined by the ability of cells to transform 3-(4,5-dimethyl-2-thiazolyl)-2,5-diphenyl. The dehydrogenase in the mitochondria of living cells can restore the yellow MTT to blue-violet [50]. Cells were seeded in 96-well culture plates (Costar) (5×10^3 cells/well) for 24 h. After incubation with the cell gradient concentration compound for 72 h, 20 μL of MTT solution per well was added to continue incubation for 4 h. A microplate reader (SpectroAmaxt 250) measures the absorbance intensity of cell growth conditions at a wavelength of 490 nm. The percent cell survival was calculated using the formula: (A_{490} of treatment group/A_{490} of untreated group) × 100%, and the IC_{50} values were procured using SPSS statistics 17.0.

4.5. The establishment of zebrafish embryo liver cancer model.

The HepG2 cells (~10^7 cells/mL) were labeled red fluorescence by DiI, which the suspended HepG2-DiI cells were injected 10–50 nL into the perivitelline space near the subintestinal vessels (SIVs) of the transgenic zebrafish (fil1:EGFP) embryos at 48 hpf by using WPI microinjector. Juvenile zebra fish of liver cancer model (48 h old) were incubated in 6-well plates (10 fishes in every well) with 2 mL solutions without or with **6** (0, 1 and 3 μM) in aquaculture water. The effect of **6** in liver cancer zebra fish were observed every 24 h with a fluorescence microscopy. The relevant ethical protocols used for the *in vivo* study for zebrafish were followed by the relevant laws.

4.6. Observation of cell ultrastructure under transmission electron microscope

Cells were harvested, precipitated, fixed with 2.5% glutaraldehyde in 0.1 mol/L PBS (pH 7.4) for 90 min, washed with cacodylate buffer, and fixed in 2% osmium tetroxide for 1 h. Then, the samples were rinsed with PBS and then gradually dehydrated in a 10% gradient series of 50%–100% ethanol and propylene oxide and embedded in Epon 812 resins. A microtome was used to create ultrathin sections, which were stained with uranyl acetate and lead citrate. Finally, the ultrastructure of the cells was observed under a transmission electron microscope.

4.7. Cell cycle and apoptosis analysis

The distribution of cells in the cell cycle phases was measured in accordance with the cellular DNA content as measured by flow cytometry with a flow cytometer (BD Biosciences). The HepG2 cells were seeded in six-well plates for 24 h and then treated with different concentrations of compound **6**. After 24 h, the floating and attached cells were collected and centrifuged before being rinsed with PBS and then fixed overnight at 4 °C with 70% ethanol. The cell cycle arrest was analyzed with an Epics XL-MCL flow cytometer (Beckman Coulter, Miami, FL, USA). The suspension was incubated with 5 μL Annexin-V-FITC and 10 μL PI for 10 min at room temperature in the dark and analyzed with an Epics XL-MCL flow cytometer (Beckman Coulter).All experiments were conducted in triplicate.

4.8. Immunofluorescence microscopy studies

The HepG2 cells seeded in six-well plates grown on coverslips were treated with drugs for 48 h and coated with poly-L-lysine. The coverslips were washed with PBS. In addition, the cells were fixed with 4% formaldehyde, permeabilized in 0.1% Triton X-100, and blocked with 4% goat serum in PBS. For LC3 staining, cells were permeabilized with 0.1% saponin. The coverslips were incubated with the primary antibody for 1 h, rinsed with PBS, and incubated with the secondary antibody for 30 min. The coverslip was washed again with PBS. After 10 min of dark-proof DAPI staining, the cells were observed under a fluorescence microscope.

4.9. DNA fragmentation analysis by agarose gel electrophoresis

The high molecular weight fragments separate by pulsed-field gel electrophoresis, and the nucleosome-sized fragments demonstrate a ladder pattern when separated on a conventional agarose gel. The DNA was prepared using a DNA extraction kit (Beyotime, Hangzhou, China). A total of 500 μL of lysis buffer containing protease was added to the cell pellet after harvesting the cells by centrifugation and then, the cells were incubated overnight at 50 °C. After digestion, the DNA was extracted by standard phenol/chloroform extraction and mixed vigorously to separate the DNA [51]. After adding ethanol and ammonium acetate and a short spin centrifugation (1 min, 12,000 rpm), the DNA was precipitated. The obtained DNA was resuspended with nuclease free water for further use. A total of 20 μL of extracted DNA was mixed with a 5 μL loading buffer (Orange G, glycerol, TAE). The samples were resolved on a 1.0% agarose gel (MP agarose, Boehringer Mannheim), and ethylene bromide staining was performed. The gel images were captured with Tanon 2500 imaging system (Shanghai, China).

4.10. Western blotting

The entire cell proteins were extracted by cell lysis buffer obtained from Cell Signaling Technology. The protein concentration was calculated by BCA assay. The proteins (20–80 μg) were separated by SDS-PAGE gel and transferred to a fixed-PVDF transfer membrane by electroblotting [52]. After blocking with 5% skim milk in TBST buffer for 1 h, the membrane was incubated with a 1:1000 diluted primary antibody in 5% skim milk powder at 4 °C overnight for subsequent washing, followed by secondary antibody incubation. Moreover, the membrane was conjugated with horseradish peroxidase for 1 h at room temperature at a 1:2000 dilution. Protein bands contain an enhanced chemiluminescence system (Tanon 4200).

Acknowledgement

This work was supported by the National Natural Science Foundation of China (Grant Nos. 81572926, 81703349). The China Postdoctoral Science Foundation (Grant No. 2017M610576). The Provincial Major Scientific Research Projects in Universities of Guangdong Province (Grant No. 2014KZDXM053), The Science and Technology Project of Guangdong Province (Grant No. 2014A020212312), The projects of Guangzhou key laboratory of construction and application of new drug screening model systems (No.201805010006) and Key Laboratory of New Drug Discovery and Evaluation of ordinary universities of Guangdong province (No. 2017KSYS002).

Conflicts of interest

The authors declare that they have no conflict of interest to disclose.

Appendix A. Supplementary material

Supplementary data to this article can be found online at https://doi.org/10.1016/j.bioorg.2019.102940.

References

[1] L.A. Torre, F. Bray, R.L. Siegel, J. Ferlay, J. Lortet-Tieulent, A. Jemal, Global cancer statistics, Ca-Cancer J. Clin. 65 (2015) (2012) 87–108.
[2] R.L. Siegel, K.D. Miller, A. Jemal, Cancer statistics, 2016, Ca-Cancer J. Clin. 66 (2016) 7.
[3] X. Adhoute, G. Penaranda, J.L. Raoul, M. Bourlière, Hepatocellular carcinoma scoring and staging systems. Do we need new tools? J. Hepatology (2016).
[4] W. Chen, R. Zheng, P.D. Baade, S. Zhang, H. Zeng, F. Bray, A. Jemal, X.Q. Yu, J. He, Cancer statistics in China(2015), Ca-Cancer J. Clin. (2016).
[5] C. Liu, Y.F. Ren, J. Dong, M.Y. Ke, F. Ma, S. Monga, R. Wu, Y. Lv, X.F. Zhang, Activation of SRY accounts for male-specific hepatocarcinogenesis: Implication in gender disparity of hepatocellular carcinoma, Cancer Lett. 410 (2017) 20.
[6] P.H. Liu, C.Y. Hsu, Y.H. Lee, When to perform surgical resection or radiofrequency ablation for early hepatocellular carcinoma? a nomogram-guided treatment strategy, Medicine 94 (2015).
[7] J. Bruix, M. Reig, M. Sherman, Evidence-based diagnosis, staging, and treatment of patients with hepatocellular carcinoma, Gastroenterology 150 (2016) 835.
[8] M.D. Julie Heimbach, L.M. Kulik, M.D. Richard Finn, C.B. Sirlin, M.D. Michael Abecassis, L.R. Roberts, A.Z.M. PhD, M.H. Murad, M.D. Jorge Marrero, Aasld guidelines for the treatment of hepatocellular carcinoma, Hepatology (2017).
[9] W.Y. Lau, E.C. Lai, The current role of radiofrequency ablation in the management of hepatocellular carcinoma: a systematic review, Ann. Surg. 249 (2009) 20–25.
[10] M.D.M.P.H. Mary Maluccio, M.D. Anne Covey, Recent progress in understanding, diagnosing, and treating hepatocellular carcinoma †, Ca-Cancer J. Clin. 622 (2012) 394–399.
[11] C.Y. Hsu, Y.H. Lee, P.H. Liu, C.Y. Hsia, Y.H. Huang, H.C. Lin, Y.Y. Chiou, F.Y. Lee, T.I. Huo, Decrypting cryptogenic hepatocellular carcinoma: clinical manifestations, prognostic factors and long-term survival by propensity score model, Plos One 9 (2014) e89373.
[12] P.H. Liu, C.Y. Hsu, C.Y. Hsia, Y.H. Lee, C.W. Su, Y.H. Huang, F.Y. Lee, H.C. Lin, T.I. Huo, Prognosis of hepatocellular carcinoma: assessment of eleven staging systems, J Hepatol (2015).
[13] C.Y. Hsu, Y.H. Lee, Y.H. Huang, C.Y. Hsia, C.W. Su, H.C. Lin, R.C. Lee, Y.Y. Chiou, F.Y. Lee, T.I. Huo, Ascites in patients with hepatocellular carcinoma: prevalence, associated factors, prognostic impact, and staging strategy, Hepatol Int 7 (2013) 188–198.
[14] H. Cao, H. Phan, L. Yang, Improved chemotherapy for hepatocellular carcinoma, Anticancer Res. 32 (2012) 1379–1386.
[15] S.H. Park, Y. Lee, H.H. Sang, S.Y. Kwon, O.S. Kwon, S.K. Sun, H.K. Ju, Y.H. Park, J.N. Lee, S.M. Bang, Systemic chemotherapy with doxorubicin, cisplatin and capecitabine for metastatic hepatocellular carcinoma, BMC Cancer 6 (2006) 243.
[16] A.E. Kayl, C.A. Meyers, Side-effects of chemotherapy and quality of life in ovarian and breast cancer patients, Curr. Opin. Obstes. Gyn. 1 (2006) 24.
[17] C.C. Sun, et al., Patient preferences regarding side effects of chemotherapy for ovarian cancer: do they change over time? Gynecol Oncol 87 (1) (2002) 118–128.
[18] F. Lozy, V. Karantza, Autophagy and cancer cell metabolism, Semin Cell Dev Bio 23 (2012) 395–401.
[19] L. Beth, Cell biology: autophagy and cancer, Nature 446 (2007) 745–747.
[20] K. Tsuchihara, S. Fujii, H. Esumi, Autophagy and cancer: Dynamism of the metabolism of tumor cells and tissues, Cancer Lett. 278 (2009) 130–138.
[21] P. Jiang, N. Mizushima, Autophagy and human diseases, Cell Res. 24 (2014) 69–79.
[22] R.K. Amaravadi, C.B. Thompson, The roles of therapy-induced autophagy and necrosis in cancer treatment, Clin. Cancer Res. 13 (24) (2007) 7271–7279.
[23] R. Amaravadi, A.C. Kimmelman, E. White, Recent insights into the function of autophagy in cancer, Gene. Dev. 30 (2016) 1913.
[24] Z. Zhong, E. Sanchez-Lopez, M. Karin, Autophagy, inflammation, and immunity: a troika governing cancer and its treatment, Cell 166 (2016) 288–298.
[25] N. Mizushima, M. Komatsu, Autophagy: renovation of cells and tissues, Cell 147 (2011) 728–741.
[26] M. Noboru, L. Beth, C. Ana Maria, D.J. Klionsky, Autophagy fights disease through cellular self-digestion, Nature 451 (2008) 1069–1075.
[27] K.N. Dalby, I.B.G. Tekedereli, B. Ozpolat, Targeting the prodeath and prosurvival functions of autophagy as novel therapeutic strategies in cancer, Int. J. Oral Sci. 13 (2015) 89–93.
[28] L. Beth, P. Milton, C. Patrice, Development of autophagy inducers in clinical medicine, J. Clin. Invest 125 (2015) 14–24.
[29] N. Santanacodina, J.D. Mancias, A.C. Kimmelman, The role of autophagy in cancer, Cancer. Bio. (2017) 19–39.
[30] A. Bergamo, G. Sava, Ruthenium complexes can target determinants of tumour malignancy, Dalton T 251 (2007) 1267–1272.
[31] E. Meggers, Targeting proteins with metal complexes, Chem. Commun. 9 (2009) 1001–1010.
[32] S. Eiji, I. Ken-Ichi, H. Tomohiro, H. Tamio, tert-Butoxide-mediated arylation of benzene with aryl halides in the presence of a catalytic 1,10-phenanthroline derivative, J. Am. Chem. Soc. 42 (2011) 15537–15539.
[33] S. Dong-Dong, W. Wei-Zhang, M. Jian-Wen, M. Wen-Jie, L. Jie, Imidazo [4,5f] [1,10] phenanthroline derivatives as inhibitor of c-myc gene expression in A549 cells via NF-κB pathway, Bioorg. Med. Chem. lett. 22 (2011) 102–105.
[34] L. Siyan, Z. Zhao, W. Qiong, W. Xicheng, M. Wenjie, Microwave-assisted synthesis of phenanthroimidazole derivatives as stabilizer of c-myc G-quadruplex DNA, Bioorg. Med. Chem. lett. 22 (2014) 6503–6508.
[35] L. Preti, O.A. Attanasi, E. Caselli, G. Favi, C. Ori, P. Davoli, F. Felluga, F. Prati, One-pot synthesis of imidazole-4-carboxylates by microwave-assisted 1,5-electrocyclization of azavinyl azomethine ylides, Eur J Org Chem (2010) 4312–4320.
[36] M.C. Mione, N.S. Trede, The zebrafish as a model for cancer, Dis. Model Mech. 3 (2010) 517–523.
[37] S.H. Lam, Z. Gong, Modeling liver cancer using zebrafish: a comparative oncogenomics approach, Cell Cycle 5 (2006) 573–577.
[38] Y. Yao, S. Sun, J. Wang, F. Fei, Z. Dong, A.W. Ke, R. He, L. Wang, L. Zhang, M.B. Ji, Q. Li, M. Yu, G.M. Shi, J. Fan, Z. Gong, X. Wang, Canonical Wnt signaling remodels lipid metabolism in zebrafish hepatocytes following ras oncogenic insult, Cancer Res. 78 (2018) 5548–5560.
[39] J. Wang, Z. Cao, X.M. Zhang, M. Nakamura, M. Sun, J. Hartman, R.A. Harris, Y. Sun, Y. Cao, Novel mechanism of macrophage-mediated metastasis revealed in a zebrafish model of tumor development, Cancer Res. 75 (2015) 306–315.
[40] M.C. Maiuri, E. Zalckvar, A. Kimchi, G. Kroemer, Self-eating and self-killing: crosstalk between autophagy and apoptosis, Nat. Rev. Mol. Cell Bio. 8 (2007) 741–752.
[41] A. Bommareddy, E.R. Hahm, D. Xiao, Atg5 regulates phenethyl isothiocyanate-induced autophagic and apoptotic cell death in human prostate cancer cells, Cancer Res. 69 (2009) 3704–3712.
[42] T.M. Nguyen, I.V. Subramanian, A. Kelekar, S. Ramakrishnan, Kringle 5 of human plasminogen, an angiogenesis inhibitor, induces both autophagy and apoptotic death in endothelial cells, Blood 109 (2007) 4793–4802.
[43] J.M. Calderón-Montaño, E. Burgos-Morón, M.L. Orta, N. Pastor, C. Perez-Guerrero, C.A. Austin, S. Mateos, M. López-Lázaro, Guanidine-reactive agent phenylglyoxal induces DNA damage and cancer cell death, Pharmacol Rep 64 (2012) 1515–1525.
[44] T. Hisatomi, N. Sueokaaragane, A. Sato, R. Tomimasu, M. Ide, A. Kurimasa, K. Okamoto, S. Kimura, E. Sueoka, NK314 potentiates antitumor activity with adult T-cell leukemia-lymphoma cells by inhibition of dual targets on topoisomerase II and DNA-dependent protein kinase, Blood 117 (2011) 3575–3584.
[45] C. Garcia-Canton, A. Anadón, C. Meredith, γH2AX as a novel endpoint to detect DNA damage: applications for the assessment of the in vitro genotoxicity of cigarette smoke, Toxicol in Vitro 26 (2012) 1075–1086.
[46] L.J. Mah, E.O.A. Tc, gammaH2AX: a sensitive molecular marker of DNA damage and repair, Leukemia 24 (2010) 679–686.
[47] H.Z. Yu, Y.Y. Jiang, Y. Fu, L. Liu, Alternative mechanistic explanation for ligand-dependent selectivities in copper-catalyzed N- and O-arylation reactions, J. Am. Chem. Soc. 132 (2010) 18078–18091.
[48] A. Shulman, G. Cade, L. Dumble, G.M. Laycock, The lethal action of 1,10-phenanthroline transition metal chelates and related compounds on dermatophytes and Candida albicans, Arzneimittel-Forsch 22 (1972) 154–158.
[49] D.M. Homden, C. Redshaw, The use of calixarenes in metal-based catalysis, Chem. Rev. 108 (2008) 5086–5130.
[50] O. Morgan, S. Wang, S.A. Bae, R.J. Morgan, A.D. Baker, T.C. Strekas, R. Engel, Two complete stereochemical sets of dinuclear ruthenium complexes, J. Chem. Soc. Dalton 20 (1997) 3773–3776.
[51] C. Lu, F. Zhu, Y.Y. Cho, F. Tang, T. Zykova, W.Y. Ma, A.M. Bode, Z. Dong, Cell apoptosis: requirement of H2AX in DNA ladder formation, but not for the activation of caspase-3, Mol. Cell 23 (2006) 121–132.
[52] M. Liu, L. Zhi, G Yee Jun, L. Yen, L. Aviva, A. Peter, Characterization of a ruthenium (III)/NAMI-A adduct with bovine serum albumin that exhibits a high anti-metastatic activity, Angew Chem. Int. Ed. 49 (2010) 1661–1664.